Retrieval of the real part of the refractive index of smoke particles from Sun/sky measurements during SCAR-B

M. A. Yamasoe,[1,2] Y. J. Kaufman,[2] O. Dubovik,[3] L. A. Remer,[3] B. N. Holben,[4] and P. Artaxo[1]

Abstract. A method is used to retrieve the real part of the refractive index of ambient aerosol particles in the entire vertical column using ground-based measurements of the angular dependence of the spectral sky radiance. The method is applied to smoke aerosol particles using spectral Sun/sky data measured by the AERONET (Aerosol Robotic Network) radiometers in Cuiabá, Brazil, during the SCAR-B (Smoke, Clouds, and Radiation–Brazil) experiment in 1995. The refractive index is retrieved from comparison between measurements taken in the solar almucantar and calculations using Mie theory. First the aerosol size distribution is derived from sky radiance at scattering angles less then 40°, then the refractive index is derived from sky radiances for angles of 20°–100°. Simulations and sensitivity studies are presented showing that the expected error is ±0.03. Application of the method to the Cuiabá region, which is dominated by smoke from cerrado vegetation burning, resulted in a mean value for the real part of the index of refraction of 1.53 ± 0.04, 1.55 ± 0.04, 1.59 ± 0.02, and 1.58 ± 0.01, respectively, for wavelengths of 438, 670, 870, and 1020 nm. Though we do not have independent verification of the results, we tested the effect of water vapor on the refractive index. The low humidification factors measured in Brazil and the lack of high relative humidities suggested a small effect of water vapor. In fact, as expected, a nonsignificant correlation was observed between the retrieved values of refractive index and total precipitable water vapor. Application to aerosol in the eastern United States (not reported here), with high humidity and high humidification factors, did show a strong reduction of the refractive index with increase of the total precipitable water vapor, thus generating confidence in the methodology.

1. Introduction

In recent years, there is an increased interest in the role of smoke aerosol particles on climate and climate change. Although concentrated in the tropics, vegetation fire, as a global activity, injects a large amount of gases and particles into the atmosphere [Crutzen and Andreae, 1990]. Smoke aerosol particles can absorb solar radiation due to the presence of black carbon particles [Andreae, 1991; Ward and Hardy, 1991; Kuhlbusch and Crutzen, 1996; Martins et al., this issue (a)] and scatter sunlight by the partially oxidized liquid organic material [Kaufman et al., this issue]. In terms of direct radiative forcing on climate, each phenomenon works in opposite direction [Hobbs et al., 1997]. Smoke particles have also an indirect effect on radiative forcing. This effect is associated with their potential to act as cloud condensation nuclei [Warner and Twomey, 1967; Hobbs and Radke, 1969; Hudson et al., 1991], including possible changes in cloud microphysics and, consequentially, cloud albedo [Kaufman and Nakajima, 1993; Kauf-

man, 1995; Heintzenberg and Wendisch, 1996; Kaufman and Fraser, 1997]. The net effect of the interaction of those particles with solar radiation remains unknown since their spatial distribution and some of their chemical and physical properties are still uncertain. The physical parameters that affect the optical properties of aerosol particles are the size distribution, index of refraction, composition (mainly the type of mixture between absorbing and nonabsorbing material) [Martins et al., this issue (a)] and shapes of the particles [Westphal and Toon, 1991; Lenoble, 1991; Penner et al., 1994]. The particle optical properties can also be affected by humidity, which may increase the particle size and decrease the index of refraction.

In this study, a modification of the method of Nakajima et al. [1983] and Wendisch and von Hoyningen-Huene [1991, 1992, 1994] is used to determine the real part of the refractive index of aerosol particles using data collected with a Sun/sky radiometer. The method involves Sun/sky measurements, which are affected directly by the aerosol optical properties in the entire atmospheric vertical column. Thus the derived index of refraction will characterize the entire column of the ambient aerosol particles, in undisturbed atmospheric conditions. Since the vertical column contains a mixture of different particles, the derived quantity is an "average" or "effective" index of refraction, hereinafter called the index of refraction for simplicity. Some simulations and a sensitivity study are presented testing the consistency and limitations of the methodology. An application for the Cuiabá site using data collected during the SCAR-B experiment is also included. Most of the biomass burning aerosol particles in this site are associated with cer-

[1]Instituto de Física, Universidade de São Paulo, São Paulo, SP, Brazil.
[2]NASA Goddard Space Flight Center Laboratory for Atmospheres, Greenbelt, Maryland.
[3]NASA GSFC and Science Systems and Applications Inc., Greenbelt, Maryland.
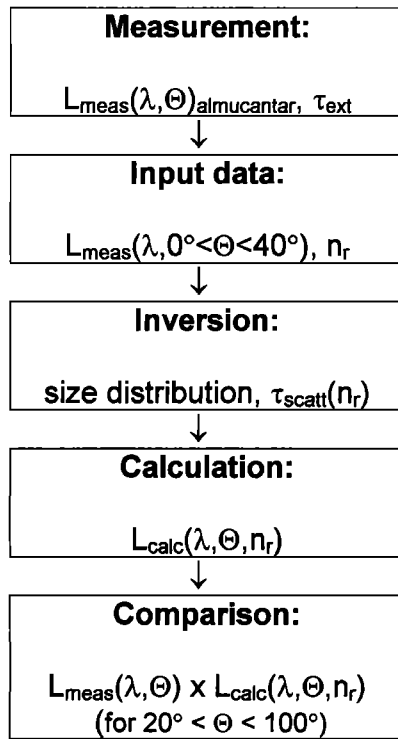[4]NASA Goddard Space Flight Center, Greenbelt, Maryland.

Measurement:

$L_{meas}(\lambda,\Theta)_{almucantar}$, τ_{ext}

↓

Input data:

$L_{meas}(\lambda,0°<\Theta<40°)$, n_r

↓

Inversion:

size distribution, $\tau_{scatt}(n_r)$

↓

Calculation:

$L_{calc}(\lambda,\Theta,n_r)$

↓

Comparison:

$L_{meas}(\lambda,\Theta) \times L_{calc}(\lambda,\Theta,n_r)$
(for 20° < Θ < 100°)

Figure 1. Summary of the adopted methodology to estimate the real part of the index of refraction (n_r) using diffuse radiance (in units of reflectance, $\pi L/F_0$) in the almucantar region measured with a Sun/sky spectral radiometer.

rado fire, although influx of aged particles from regions dominated by forest fires is also possible [*Remer et al.*, this issue].

2. Methodology

The study is based on the minimization of error in the comparison between measured angular distribution of diffuse solar radiation (in reflectance units, $\pi L/F_0$) and a calculated one, varying the real part of the refractive index. Figure 1 summarizes the basic principle. The measurements of direct and diffuse spectral solar radiation were carried out using the AERONET automatic Sun/sky scanning radiometer in the almucantar region [*Holben et al.*, 1996].

To calculate the diffuse solar radiation, information on size distribution and aerosol optical thickness of the particles are required. Size distribution was retrieved using an inversion scheme proposed by *Nakajima et al.* [1983] and applied to sky data for the wavelengths of 438, 670, 870, and 1020 nm, simultaneously, varying the real part of the refractive index. With the retrieved size distribution the Nakajima inversion code also estimates the scattering aerosol optical thickness (τ_{scatt}). From direct sunlight measurements, extinction aerosol optical thickness can be derived according to the Beer-Lambert-Bouger attenuation law [*Schmid and Wehrli*, 1995], after correction of gas absorption and molecular scattering through the Langley plot method:

$$V(\lambda) = V_0(\lambda)R^{-2}\exp[-m(\theta_0)\tau(\lambda)] \qquad (1)$$

where $V(\lambda)$ is the output voltage of the Sun photometer obtained when the directly transmitted solar irradiance is observed over a small bandpass $\Delta\lambda$ centered at wavelength λ_0;

$V_0(\lambda)$ is the instrument calibration constant or the output voltage measured at the top of the atmosphere; R is the Earth-Sun distance in astronomical units at the time of observation (formula taken from *Iqbal* [1983]); $\tau(\lambda)$ is the spectral optical thickness; $m(\theta_0)$ is the relative optical air mass; and θ_0 is the solar zenith angle.

Furthermore, the four wavelengths were carefully selected to avoid strong gas absorption. The only slight gas absorption is due to ozone. Rewriting (1) in terms of each attenuator,

$$V(\lambda) = V_0(\lambda)R^{-2}$$
$$\cdot \exp[-m_r(\theta_0)\tau_r(\lambda) - m_o(\theta_0)\tau_o(\lambda) - m_a(\theta_0)\tau_{ext}(\lambda)]$$
$$(2)$$

where $m_r(\theta_0)$ is the Rayleigh relative optical air mass obtained from *Kasten and Young* [1989]; $\tau_r(\lambda)$ is the Rayleigh optical depth derived from *Bucholtz* [1995]; $m_o(\theta)$ is the ozone optical air mass from *Komhyr et al.* [1989]; $\tau_o(\lambda) = k_o(\lambda)C_o$ is the O_3 optical depth, with $k_o(\lambda)$ the ozone absorption coefficient taken from *Vigroux* [1953] and C_o the ozone column amount obtained from *London et al.* [1976]; $m_a(\theta_0)$ is the aerosol optical air mass obtained from *Kasten and Young* [1989], and $\tau_{ext}(\lambda)$ is the aerosol optical thickness.

The difference between the extinction aerosol optical thickness (τ_{ext}) from direct measurement and τ_{scatt} derived from the inversion of sky radiances is used to estimate the single-scattering albedo [*Dubovik et al.*, this issue], a measure of the aerosol absorption mainly by black carbon. The size distribution, the estimated scattering aerosol optical thickness, and black carbon absorption for a particular value of the real part of the index of refraction are input in a full radiative transfer code of *Dave and Gazdag* [1970] to calculate the downward irradiance in the almucantar. This code assumes a plane parallel atmosphere with homogeneous spherical Mie particles. Note that there are some differences between Dave code for forward calculations and Nakajima inversion code. In the Dave code, an atmosphere with a vertical structure consisting of up to 160 homogeneous layers is simulated, whereas in the Nakajima code, only one homogeneous atmospheric layer was used. Furthermore, the treatment of multiple scattering in the Dave code is based on a modified Fourier transform method [*Dave and Gazdag*, 1970], while the Nakajima code uses the discrete ordinate method and the truncation approximation [*Nakajima et al.*, 1983; *Nakajima and Tanaka*, 1988]. Only sky radiance data for a scattering angle of 3°–40° were used in the inversion of size distribution (no measurements are possible for angles smaller than 3°). In this angular region the dominant scattering effect is diffraction of light, which depends on the size of the particles and is independent of the index of refraction and composition [*van de Hulst*, 1981; *Kaufman et al.*, 1994]. Also, the differences between spheres and nonspherical particles with equal area are negligible at forward scattering angles [*West et al.*, 1997], and the effect of multiple scattering and reflection from the Earth surface are smaller in this region than for higher scattering angles [*Kaufman et al.*, 1994].

The predominant absorber in smoke aerosol is black carbon particles which are very small spheres of about 0.05 μm in diameter arranged in clusters, [*Martins et al.*, this issue (b)]. According to *Bohren and Huffman* [1983], because of their small sizes, black carbon particles present a very small scattering cross section and can be considered as pure absorbing particles. The way those particles are mixed with the organic component is not very clear, and probably several mixing ge-

Table 1. Input Parameters Used to Simulate Angular Distributions of Intensities in Dave Code

Index of Refraction	Lognormal Parameters				
	r_g(acc), μm	σ(acc)	r_g(coa), μm	σ(coa)	N_1/N
1.50–0i	0.0448	0.60	0.0982	1.26	0.9988

Index of refraction and lognormal parameters. $N = N_1 + N_2$.

Figure 2. Original and retrieved volume size distributions with different values of the real part of the refractive index.

ometries are possible. For simplicity, a model for light extinction by an external mixture of black carbon and organic particles is assumed. In this model, the organic particles are assumed as pure scatterer with a null imaginary part of the index of refraction. This assumption is justified since black carbon surrounded by nonabsorbing material has a similar phase function to the particles of the nonabsorbing material alone [*Ackerman and Toon*, 1981]. In such a model, black carbon is considered the only absorber and the organic material the only scatterer with a complex index of refraction n_r − $0.0i$, where n_r is the real part of the index of refraction to be determined by the proposed methodology.

The comparison between the measured and the calculated scattered solar radiation was performed in the angular interval of $20° < \Theta < 100°$. According to simulations the influence of the index of refraction is important only for angles larger than $20°$, as will be shown in this paper. Moreover, angles $\Theta > 100°$ were not used to minimize the effects of uncertainties in surface reflectance [*Wendisch and von Hoyningen-Huene*, 1992] (and also shown in this paper in the sensitivity study section) and possible particle nonsphericity. The best fit between measured (L_{meas}) and calculated (L_{calc}) radiances was considered the one presenting the minimum root-mean-square-error in the logarithmic space (RMSELS), defined as

$$\text{RMSELS} = \sqrt{\frac{1}{N} \sum_{i=1}^{N} \{\ln [L_{meas}(\Theta_i)] - \ln[L_{calc}(\Theta_i)]\}^2} \quad (3)$$

The physical interpretation of the root-mean-square-error of the logarithm of the radiance is associated to its relative error, as can be shown for small errors:
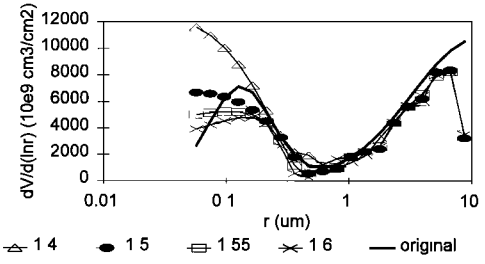
Suppose that

$$L_{calc} = L_{meas} + \Delta L \quad (4)$$

then

$$|\ln (L_{meas}) - \ln (L_{calc})| \approx \left|\frac{\Delta L}{L}\right|, \quad \text{for } \Delta L \to 0 \quad (5)$$

In terms of statistical estimation theory the use of logarithmic errors is equivalent to the assumption of lognormal noise, which characterizes the random error of positively defined values [*Dubovik et al.*, 1995] (sky radiance is nonnegative by its physical nature). Thus it is assumed that the errors in measured radiance are distributed lognormally, statistically independent, and equal.

3. Simulations

The methodology to derive the refractive index was developed using simulations of scattered intensities of solar radiation. To perform the simulations, a two mode lognormal size distribution representing the accumulation (acc) and the coarse (coa) modes was used. Table 1 lists the parameters of the distribution given by

$$\frac{dN}{dr} = \frac{N_1}{\sqrt{2\pi}\sigma(acc)} \exp\left\{\frac{-[\ln (r/r_g(acc))]^2}{2\sigma^2(acc)}\right\}$$
$$+ \frac{N_2}{\sqrt{2\pi}\sigma(coa)} \exp\left\{\frac{-[\ln (r/r_g(coa))]^2}{2\sigma^2(coa)}\right\} \quad (6)$$

The properties of the atmosphere used in the simulation are presented in Table 2. The spectral surface reflectances used are the same as measured at Cuiabá, and a solar zenith angle (θ_0) of $60°$ was chosen. The simulations of the scattered solar intensities were generated using the code of *Dave and Gazdag* [1970] discussed previously. Using the generated scattered intensities of radiation, volume size distributions were retrieved using the fast inversion code of *Nakajima et al.* [1983, 1986], changing the real part of the index of refraction. Figure 2 presents the original and retrieved size distributions. From the figure, it is possible to observe that even using data for an angular region where the influence of the index of refraction is minimum, some dependence on refractive index is still observable, especially for the accumulation mode particles. The retrievals are consistent with the original size distribution model. To confirm the consistency between the independent codes, new scattered radiances were calculated using the retrieved

Table 2. Spectral Parameters of Simulated Atmosphere Including Rayleigh, Ozone and Water Vapor Optical Thicknesses, and Surface Reflectance

λ	438 nm	670 nm	870 nm	1020 nm
$\tau_{Rayleigh}$	0.2396	0.0424	0.0146	0.0077
τ_{ozone}	0.00	0.013	0.00	0.00
τ_{water}	0.00	0.00	0.00	0.00
Surface reflectance	0.07	0.15	0.25	0.25

Table 3. Retrieved Values of Real Part of Index of Refraction (n_r) Using Simulated Data

λ, nm	438	670	870	1020
n_r	1.495	1.499	1.498	1.494
Minimum RMSELS	0.013	0.007	0.021	0.034

The minimum value of the root mean square error is also presented for each considered wavelength. Original value was $n_r = 1.50$.
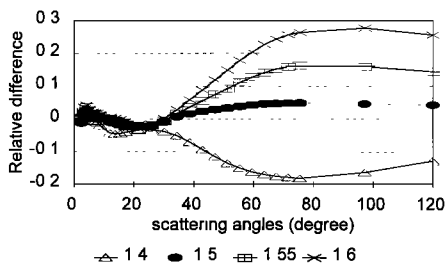
Figure 3. Relative differences of scattered intensities of radiation ($[L_{ret} - L_{ori}]/L_{ori}$) for different real part of the refractive index. Plots for wavelength of 1020 nm.

size distributions in the radiative transfer code of *Dave and Gazdag* [1970]. The methodology to derive the real part of the index of refraction was applied, and the results are presented in Table 3. In this case, no additional errors were added, and the methodology retrieved accurately the index of refraction of 1.5. The maximum absolute difference from the true refractive index was 0.006, detected for the wavelength of 1020 nm, for which the minimum value of the RMSELS was also the highest. In order to illustrate the angular region where the radiance is sensitive to the index of refraction, relative differences between the original and the retrieved scattered radiances were plotted in Figure 3 for the wavelength of 1020 nm. The figure shows that the sky radiance is sensitive to the index of refraction for scattering angles larger than 20°. A change in refractive index of 0.05 generates a change in radiance of more than 10%, for the considered wavelength, as can be observed in Figure 3. The departure from zero of the curve calculated using the correct index of refraction (1.5) is attributed to the difference between the two codes. Better results were observed for the other wavelengths. As previously mentioned, the tests for 1020 nm presented the greatest errors. Therefore it can be concluded that the two codes were compatible, the method to derive the refractive index is not sensitive to the differences between the codes, and the codes can be used in this study.

4. Sensitivity Study

In this section, results of a sensitivity study to uncertainties in some of the input parameters are discussed. The sensitivity study was applied to investigate the consistency and limitations of the proposed methodology. The approach is considered successful or consistent if the difference between the retrieved and the true index of refraction, Δn_r, is smaller than ±0.015. Without introducing an additional error, for scattering angle Θ

Table 4. Best Estimates of True Index of Refraction by Described Methodology Using a Different Value of Solar Zenith Angle in Retrieval of Size Distribution and Posterior Scattered Radiation, Original $\theta_0 = 60°$

Wavelength, nm	438	670	870	1020
New Solar Zenith Angle = 61.3° (Nakajima), 62° (Dave)				
n_r	1.509	1.486	1.493	1.486
Minimum RMSELS	0.025	0.024	0.025	0.015
New Solar Zenith Angle = 58.6° (Nakajima), 58° (Dave)				
n_r	1.489	1.507	1.506	1.504
Minimum RMSELS	0.010	0.020	0.008	0.014

< 20° (where the influence of the refractive index is small) the maximum relative difference observed between the original and the retrieved scattered radiances is <5% for all the values of refractive indices. In the angular region where the radiance is sensitive to the refractive index (30° < Θ < 90°), a 5% maximum relative difference in the sky radiance was obtained only by restricting the refractive index to 1.500 ± 0.015.

The influence of errors in the accuracy of pointing to the Sun (simulated by an error in solar zenith angle of 2°) and errors in the surface reflectance on the methodology was tested. The analysis was also carried out to verify the sensitivity of the approach to random (statistical) and calibration (systematic) errors in the angular distribution of the scattered radiances. The systematic error of 2° in the solar zenith angle is also used to test if variation in the position of the Sun during the measurement sequence could affect the analysis. The simulated sky radiances for solar zenith angle of 60° were used for retrievals of size distributions using the Nakajima code for several different values of the solar zenith angle. With the retrieved size distributions, new calculations of radiances were performed in the Dave code using a new solar zenith angle, 2° apart from the original input. The summary of the sensitivity to error in the solar zenith angle is presented in Table 4. The results show that errors in solar zenith angle of the order of 2° do not influence the reliability of the methodology, according to the chosen consistency threshold. The used values for the solar zenith angles in Nakajima and Dave codes in the retrievals are distinct due to a limitation in the Dave code. Only even numbers are accepted in the Dave code as input for solar zenith angle. Thus a maximum departure from the original value of 2° was inserted in the retrievals also to verify the importance of this limitation on the results. The differences between the original and retrieved radiances were significant only in the forward direction (for scattering angles smaller than 10°). Therefore the methodology to retrieve the real part of the index of refraction is insensitive to this kind of error. In reality, the error in pointing to the Sun is <0.5°. The measurement sequence in the almucantar takes less than 200 s for the four wavelengths, resulting in a change of the Sun's position of less than 0.85°.
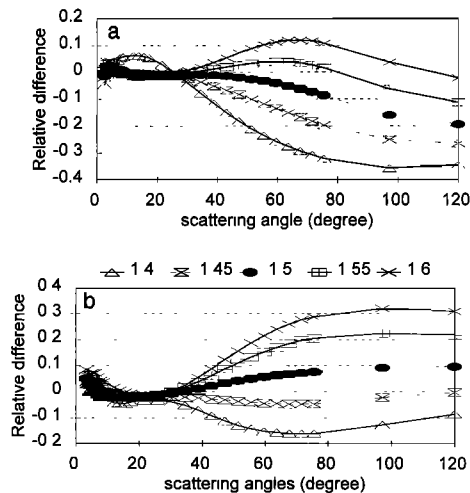

Figure 4. Relative differences of scattered intensities of radiation ($[L_{ret} - L_{ori}]/L_{ori}$) for different real part of the refractive index. Plots for wavelength of 1020 nm, with errors in surface reflectance. (a) Null surface reflectance. (b) Surface reflectance 30% higher than original.

Sensitivities of the method to errors in surface reflectance are shown in Figures 4a and 4b. They present plots of the relative difference between the original scattered intensity and the retrieved intensities after altering the value of surface reflectance for the four wavelengths. In Figure 4a, plots for 1020 nm using null surface reflectance are shown. Figure 4b corresponds to the case where surface reflectance is overestimated by about 30% of the original values. Figure 4a shows that all the radiance differences become negative as the scattering angle increases. The opposite trend can be seen from Figure 4b. The same pattern was observed for the four wavelengths. Table 5 summarizes the retrieved indices of refraction for these cases. Other analyses are also included in the summary: underestimation of surface reflectance by about 50% of the original values and retrievals with surface reflectance with a different spectral dependence. The last analysis was carried out to evaluate the influence of the spectral dependence of surface reflectance on the methodology.

From this study, it is possible to conclude that surface reflectance significantly affects the angular dependence of the scattered radiances, and therefore knowledge of the surface reflectance is important to the determination of the real part of the index of refraction. Although the RMSELS values for some cases with wrong surface reflectance are smaller than the case with no error involved, the retrieved index of refraction is out of the consistency limits due to the erroneous angular pattern produced. Radiances in longer wavelengths appeared to be more sensitive to errors in surface reflectance. Accuracy better than 30% in the determination of surface reflectance would be required to derive reliable indices of refraction. With 30% of error, only the retrieval of the index of refraction at 1020 nm was out of the considered threshold, as observed in

Table 5. Best Estimates of Index of Refraction and Respective Minimum RMSELS by Described Methodology Using Different Values of Surface Reflectance in Retrieval of Size Distribution and Posterior Scattered Radiation

Wavelength, nm	Surface Reflectance	n_r	Minimum RMSELS
Zero Surface Reflectance			
438	0 00	1.496	0 008
670	0.00	1.519	0.033
870	0 00	1.544	0.031
1020	0.00	1.544	0 029
50% of the Original			
438	0.035	1.495	0.011
670	0.075	1.508	0.014
870	0.125	1.516	0.025
1020	0 125	1.514	0.018
Different Spectral Dependence			
438	0.05[a]	1.501	0.012
670	0.08[b]	1.510	0.015
870	0.15[c]	1.515	0.019
1020	0.20[d]	1.506	0.021
30% Higher Than Original			
438	0.090	1.494	0.014
670	0.195	1.496	0.016
870	0.320	1.490	0.034
1020	0.330	1.483	0.049

[a]70% of the original.
[b]53% of the original.
[c]Equal the original.
[d]80% of the original.

Table 6. Retrieved Real Part of Index of Refraction and Minimum RMSELS With Inclusion of Statistical and Systematic Errors in Scattered Radiances

Wavelength, nm	438	670	870	1020
Statistical Error in L				
n_r	1.488	1.499	1.479	1.494
Minimum RMSELS	0.034	0.030	0.058	0.045
Systematic Error				
Calibration off by	+7%	+7%	+7%	+7%
n_r	1.468	1.487	1.484	1.479
Minimum RMSELS	0.010	0.019	0.030	0.035
Calibration off by	+2%	-2%	+5%	-8%
n_r	1.459	1.479	1.521	1.459
Minimum RMSELS	0.015	0.032	0.029	0.025
Calibration off by	+5%	+3%	+1%	+1%
n_r	1.486	1.493	1.485	1.478
Minimum RMSELS	0.015	0.024	0.030	0.021

Table 5. Thus for smaller errors the methodology might be consistent for all wavelengths. Comparing Figures 3 and 4, it is noticed that the effect of refractive index on the radiance relative difference is distinct from the effect of error in surface reflectance. The first generates only a small angular dependence in the relative difference when the correct index of refraction is used and the second a significant angular dependence.

The next test is related to the influence of errors in the scattered intensities of radiation on the method. Random errors in the radiances were generated with a Gaussian distribution of mean zero and standard deviation of 12% for scattering angles $\Theta < 10°$ and 5% for the other angular region. The test for calibration error was performed assuming an equal displacement for the four wavelengths and also altering each wavelength by a different amount (positive or negatively), randomly chosen. Table 6 presents the results.

The inclusion of random errors in the scattered intensities of radiation did not affect significantly the retrieved refractive index. The only exception was observed for the wavelength of 870 nm, for which the retrieval of the index of refraction was lower than permitted by the considered threshold. Maximum observed errors in the instrumentation are of the order of 5% due to random errors. On the other hand, well-calibrated instrumentation is required to avoid incorrect retrievals of the real part of the index of refraction. Figure 5 illustrates an example of the influence of calibration error in the scattered radiances for the wavelength of 1020 nm, using errors of +2,
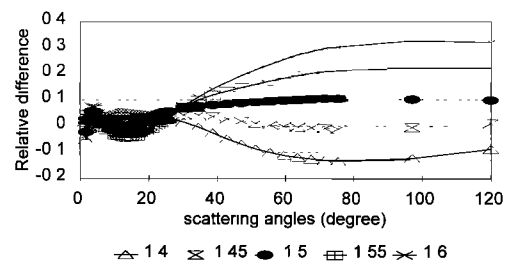

Figure 5. Relative differences of scattered intensities of radiation ($[L_{ret} - L_{ori}]/L_{ori}$) for different real part of the refractive index. Plots for wavelength of 1020 nm, simulating a calibration error of +2, −2, +5, and −8% for the channels 438, 670, 870, and 1020 nm, respectively.

Table 7. Values of Spectral Aerosol Optical Thicknesses, Precipitable Water Vapor, and $\alpha(870,438)$ for Data Used to Retrieve Real Part of Index of Refraction

1995	Time, GMT	AOT				Precipitable Water, cm	α (870,438)
		438	670	870	1020		
August 7	1137	0.4038	0.1813	0.1178	0.0889	2.736	−1.7951
August 10	1112	0.2995	0.1272	0.0877	0.068	1.650	−1.7897
August 13	2008	0.4599	0.2009	0.1245	0.0923	1.992	−1.9041
August 14	1132	0.3592	0.1468	0.0959	0.0693	1.808	−1.9243
	2008	0.2447	0.1028	0.0725	0.0566	1.524	−1.7725
August 17	2009	0.4934	0.2531	0.1726	0.1328	2.206	−1.5305
August 18	1922	0.5364	0.2624	0.1833	0.1398	2.384	−1.5646
	2010	0.5109	0.2530	0.1740	0.1365	2.450	−1.5695
August 19	1923	0.4771	0.2301	0.1662	0.1289	2.412	−1.5366
	2010	0.4225	0.2111	0.1525	0.1237	2.535	−1.4849
August 20	1128	0.4048	0.2034	0.1487	0.1210	2.544	−1.4593
	1923	0.3650	0.1740	0.1289	0.1007	2.284	−1.5167
	2010	0.3886	0.1910	0.1372	0.1110	2.430	−1.5171
August 23	1924	0.3234	0.1459	0.1108	0.0865	1.765	−1.5608

Shown also the date and time of measurement.

−2, +5, and −8% for the wavelengths of 438, 670, 870, and 1020 nm, respectively, to retrieve size distributions. From the figure, it is possible to observe a 5–10% shift from zero of the correct index of refraction (in this case, 1.50). Table 6 shows that for the case using a same error of 7%, the methodology retrieves indices of refraction out of the considered threshold ($n_r = 1.500 \pm 0.015$) for all the wavelengths, although the obtained RMSELS values were small. Calibration errors of the sky radiances are of the order of 5% maximum. To test the effect of a spectrally varying calibration error limited by 5%, errors of 5, 3, 1, and 1%, respectively, for the channels 438, 670, 870, and 1020 nm are simulated. Simulations for these errors showed that the methodology is consistent except for the 1020 nm channel, for which the retrieved index of refraction was out of the chosen limits, as seen in Table 6.

The sensitivity study showed that the minimum observed RMSELS was smaller than 0.06. For this reason, in the application to measurements, cases where the index of refraction was derived with a minimum RMSELS larger than 0.06 were not taken into account. For the simulated calibration errors the method was inconsistent only for the retrieval of the index of refraction for 1020 nm, when the scattered radiances have a maximum error in calibration of 5%. For larger calibration errors an incorrect index of refraction is derived. Therefore the application of the method to the analysis of real cases should be consistent, assuring that no larger calibration errors are involved. Surface reflectance uncertainties influence the scattered radiances for larger scattering angles. The greater the inaccuracy, the stronger the influence, affecting the angular behavior of the radiances. For this reason the angular behavior of the relative differences between the measured and the calculated scattered radiances were monitored for each analyzed case, even when the minimum RMSELS $\leq$ 0.06.

5. Application to Measurements

Sky measurements were collected from August 7 to 23, 1995, at a Cuiabá site, located in Mato Grosso state, at the southern portion of the Amazon Basin. As mentioned previously, the site is dominated by the presence of smoke from cerrado biomass burning with some events of aged smoke advected to the region from forest fires farther North. The combustion process

of cerrado vegetation occurs mainly in flaming conditions [Ward et al., 1992; Kauffman et al., 1994], with the production of high concentrations of very small soot particles which subsequently aggregate to form large-particle clusters [Martins et al., this issue (b)]. Fresh clusters can be up to tens of microns in size and assume various shapes. On the other hand, forest combustion is dominated by smoldering processes [Ward et al., 1992], with emission of nearly spherical particles. Another important source of large particles at Cuiabá site is soil dust, specially during the dry season, which coincides with the burning period [Echalar et al., this issue]. Size distributions obtained from this site through inversion of almucantar data collected during the SCAR-B period presented a bimodal pattern [Remer et al., this issue].

Measurements of the sky radiances in the Sun's almucantar were carried out once per hour in the morning and late afternoon when the solar zenith angle was greater than 58° up to 76°, approximately [Holben et al., 1996]. The measurements were performed by one of the Aerosol Robotic Network (AERONET) ground-based narrowband Cimel Sun-sky scanning spectral radiometers [Holben et al., 1996, 1998]. The almucantar is the region of the sky where the view zenith angle (θ) is equal to the solar zenith angle (θ_0). Measurements are taken in a conical surface with varying azimuth angle (φ) relative to the Sun. In this geometry the scattering angle Θ is related to θ_0 and φ by the expression $\cos \Theta = \cos^2 \theta_0 + \sin^2 \theta_0 \cos \varphi$. The sky radiances from both sides of the Sun were averaged, and asymmetrical almucantars were not considered. The asymmetry is due to atmospheric inhomogeneities or the presence of clouds. The measurements were performed with azimuth angle steps of 0.5° from 3° to 4°, of 1° from 4° to 8°, 2° from 8° to 20°, of 5° from 20° to 50°, 10° from 50° to 100°, and of 20° from 100° to 180°. The same angular resolution was used in the retrievals of size distribution but in the interval 3°–40° and in the posterior comparisons of scattered radiances (taking angles between 20° and 100°). The radiances were normalized by the solar flux to derive the radiances in units of reflectance ($\pi L/F_0$).

With the same instrumentation, precipitable water vapor amount is derived from a modified Langley plot algorithm using the 940 nm water vapor absorption band [Bruegge et al.,

Table 8. Retrieved Real Part of Index of Refraction and Respective Minimum RMSELS Observed

1995	Time, GMT	438 nm		670 nm		870 nm		1020 nm	
		n_r	Minimum RMSELS	n_r	Minimum RMSELS	n_r	Minimum RMSELS	n_r	Minimum RMSELS
August 7	1137	1.475	0.020	1.512	0.026	1.553	0.038	*	*
August 10	1112	1.562	0.013	*	*	*	*	*	*
August 13	2008	1.513	0.016	1.600	0.030	1.600	0.026	1.600	0.036
August 14	1132	*	*	1.521	0.026	*	*	*	*
	2008	1.592	0.028	1.569	0.019	*	*	*	*
August 17	2009	1.497	0.013	1.562	0.019	1.598	0.034	1.586	0.040
August 18	1922	1.535	0.019	1.542	0.013	1.581	0.019	1.568	0.031
	2010	1.509	0.006	1.562	0.013	1.590	0.022	1.578	0.052
August 19	1923	1.540	0.020	1.524	0.021	*	0.031	*	0.047
	2010	1.535	0.013	1.581	0.022	*	*	*	*
August 20	1128	*	*	1.570	0.039	*	*	*	*
	1923	1.578	0.021	1.580	0.017	*	*	*	*
	2010	1.532	0.011	1.589	0.015	*	*	*	*
August 23	1924	*	*	1.472	0.021	1.585	0.040	1.586	0.041

Applications to measurements in Cuiabá during SCAR-B.
*Minimum RMSELS was higher than 0.06 or angular distribution of relative differences of scattered radiation exhibited a singular behavior (see text).

1992; *Halthore et al.*, 1997] and coefficients from the LOWT-RAN-7 code. Comparisons made between precipitable water vapor retrieved from CIMEL and radiosonde and/or microwave retrievals have shown differences typically of the order of 5-10% (T. F. Eck, personal communication, 1997). In addition to that, a measure of the particle size, the wavelength exponent or Ångström exponent α [*Kaufman et al.*, 1992; *King et al.*, 1978] is calculated from the wavelength dependence of the aerosol optical thickness

$$\alpha(\lambda_1, \lambda_2) = \frac{\ln\,(\tau_1/\tau_2)}{\ln\,(\lambda_1/\lambda_2)} \quad (7)$$

The more negative the value of α the smaller the overall size of the particles. Spectral aerosol optical thicknesses for the four wavelengths, precipitable water vapor and the Ångström exponent calculated for 438 and 870 nm wavelengths, $\alpha(870,438)$, for the considered cases are presented in Table 7. In Table 8 the retrieved real part of the index of refraction is listed with the observed minimum RMSELS values. The retrieved indices of refraction for the channels 438 nm and 670

nm were plotted against the precipitable water vapor in Figure 6. It is possible to observe that there is a slight negative correlation between the real part of the index of refraction for the wavelength of 438 nm ($R^2 = 0.42$, where R^2 is the fraction of the variance of the dependent variable explained by the linear fit), although no similar pattern could be observed for the retrievals of the 670 nm wavelength ($R^2 = 0.02$). Similar behavior was observed between those variables and the aerosol optical thickness for 438 nm: $R^2 = 0.42$ for $n_r(438)$ and $R^2 = 0.01$ for $n_r(670)$. In the same figure, the size distribution is evaluated as a function of the amount of precipitable water vapor present in the column, through the $\alpha(870,438)$ exponent, presenting a poor correlation. This small effect of humidity is in agreement with measurements of humidification factor during SCAR-B performed by *Kotchenruther and Hobbs* [this issue]. In their work it was observed that aerosol particles from biomass burning present a small humidification factor, compared to urban particles, meaning a smaller hygroscopic growth. The fact that the index of refraction retrieved from real atmospheric conditions does not present large variations with the amount of precipitable water reinforces this observation.

Table 9 presents the mean values and standard deviations of the retrieved real part of the index of refraction for the cases analyzed in this work, for the four wavelengths. Reported values for the real part of the refractive index for smoke aerosol particles in the literature are scarce. *Westphal and Toon* [1991] used a value of 1.55 for the 0.5 μm wavelength in simulations of forest fire smoke plume, using a numerical model. *Anderson et al.* [1996] and *Lenoble* [1991] used a value of 1.52 in their studies of smoke optical properties.
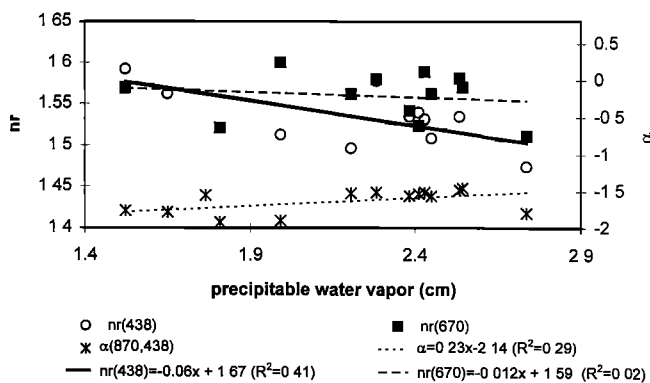

Figure 6. Real part of the indices of refraction for the wavelengths 438 and 670 nm and α exponent (or wavelength exponent) as functions of precipitable water vapor. R^2 is the fraction of the variance of the dependent variable explained by the linear fit.

Table 9. Spectral Mean Values and Standard Deviations for Real Part of Index of Refraction for Studied Cases

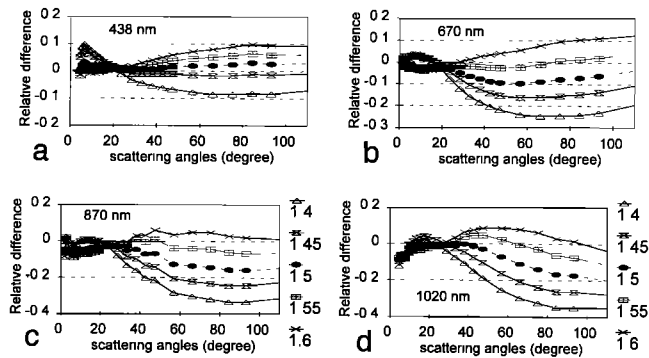| Wavelength, nm	438	670	870	1020
Mean n_r	1.533	1.553	1.585	1.584
Standard deviation	0.035	0.036	0.017	0.012
Number of data	11	13	6	5

Figure 7. Relative difference between measured and calculated scattered radiances for distinct values of the real part of the refractive index. Data were taken at Cuiabá on August 17, 1995, at 2009 GMT. (a) 438 nm, (b) 670 nm, (c) 870 nm, and (d) 1020 nm.

As observed from Table 8, the determination of the real part of the index of refraction for larger wavelengths was not always possible. In general, the behavior of the retrieved scattered radiances was distinct from the original for larger scattering angles, presenting a similar pattern as if the surface reflectance were underestimated. Figure 7 shows an example for which the retrievals were successful, although the pattern is already observable for the 1020 nm wavelength. In Figure 8 an example for which the singular behavior in the angular distribution of the relative differences was observed for larger wavelengths is presented. The physical explanation for such behavior is still under investigation. The possibility of an underestimated surface reflectance or calibration problems is unlikely. The analyzed data presented in this work were collected using the same instrument for which good retrievals were possible. To explain this angular dependence, a surface reflectance value 2–3 times higher than the considered would be necessary. Such strong variation in surface reflectance in only a few days is improbable. One possible explanation for that behavior is the presence of the large nonspherical mineral dust particles. In the presence of such kind of particles, Mie theory may not be valid [*Mishchenko and Travis*, 1994; *Mishchenko et al.*, 1997]. Figures 9 show the contribution of the coarse mode particles to the normalized radiance considering only single scattering (τ_{scatt} times phase function). Figure 9a was generated using the size
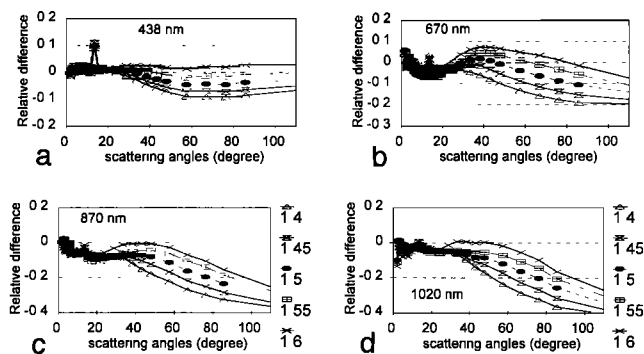

Figure 8. Relative difference between measured and calculated scattered radiances for distinct values of the real part of the refractive index. Data were taken at Cuiabá on August 10, 1995, at 1112 GMT. (a) 438 nm, (b) 670 nm, (c) 870 nm, and (d) 1020 nm.
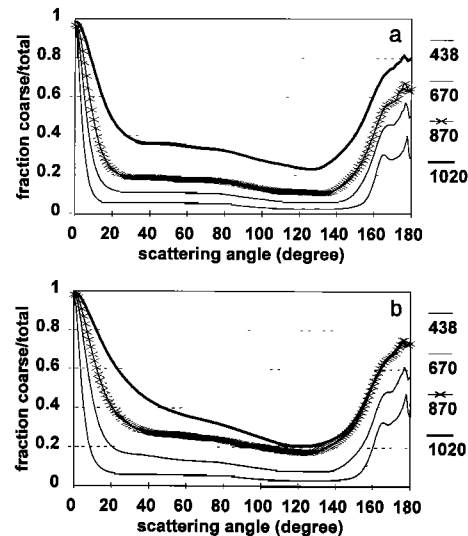

Figure 9. Contribution of the coarse mode particles to the nonnormalized phase function as function of scattering angle and wavelength. Calculations performed using retrieved size distribution and the real part of the index of refraction for (a) August 17, 1995, 2009 GMT and (b) August 10, 1995, 1112 GMT.

distribution retrieved with sky radiances collected on August 17, 1995, and Figure 9b with data from August 10, 1995. The importance of the coarse mode becomes more significant as the wavelength increases in the angular range 20° < Θ < 100° (range considered in the retrieval of the index of refraction). Comparing Figures 9a and 9b, it is possible to observe that for August 17 the contribution of the coarse mode particles to the normalized radiance (calculated for demonstration purposes using single scattering) is significant only for 1020 nm (>20%). On the other hand, for August 10 the importance of the coarse mode is also observable for 870 nm, reaching up to 60% for 1020 nm. Moreover, the decrease of this contribution is less dependent on the scattering angle for the last case than for the preceding one. Such high contribution of coarse mode particles to the radiance at longer wavelengths indicates the possible effect of nonsphericity of the large particles on the sky radiances. Mie theory, used in the present method seems to be consistent only for retrievals of the real part of the index of refraction at shorter wavelengths.

6. Conclusions

A method is developed to retrieve the real part of the refractive index of aerosol particles in undisturbed, ambient conditions. A sensitivity study shows that well-calibrated radiometers and knowledge of spectral surface reflectance with a precision better than 30% are required to derive the refractive index within an error of ±0.03. From the investigation of measurements at Cuiabá, it was observed that smoke aerosol particles present in the region have a mean value of the real part of the index of refraction of 1.55 ± 0.04 at 670 nm. The influence of the precipitable water vapor on the index of refraction was found to be negligible, although a small reduction of the real part of the index of refraction for the 438 nm wavelength was observed. This was expected due to the low-humidification factors measured in Brazil and the lack of high humidities during the dry season. Note that derivation of the

refractive index of aerosol in the eastern United States, not reported in this paper, did show a strong reduction of the refractive index with increase of the total precipitable water vapor. This region has high humidities during the summer measurement period, and the aerosol has high-humidification factors due to the presence of sulfates. These water vapor dependencies of the retrieved refractive index generate confidence in the methodology. The mean values of the derived refractive indices for the other channels are 1.53 ± 0.04 for 438 nm, 1.59 ± 0.02 for 870 nm, and 1.58 ± 0.01 for 1020 nm. The derivation of the refractive index for 1020 nm is uncertain, probably because of the effect of large soil particles that may be nonspherical. Other cases from the same site and from sites dominated by forest fire smoke will also be analyzed to get a temporal and spatial characterization of the real part of the index of refraction of smoke aerosol particles.

References

Ackerman, T. P., and O. B. Toon, Absorption of visible radiation in atmosphere containing mixtures of absorbing and nonabsorbing particles, *Appl. Opt., 20,* 3661–3668, 1981.

Anderson, B. E., W. B. Grant, G. L. Gregory, E. V. Browell, J. E. Collins Jr., G. W. Sachse, D. R. Bagwell, C. H. Hudgins, D. R. Blake, and N J. Blake, Aerosols from biomass burning over the tropical South Atlantic region: Distributions and impacts, *J. Geophys. Res., 101,* 24,117–24,138, 1996.

Andreae, M. O., Biomass burning: Its history, use and distribution and its impact on environmental quality and global climate, in *Global Biomass Burning—Atmospheric, Climatic, and Biospheric Implications,* edited by J. S. Levine, pp. 3–21, MIT Press, Cambridge, Mass., 1991.

Bohren, C. F., and D. R. Huffman, *Absorption and Scattering of Light by Small Particles,* John Wiley, New York, 1983.

Bruegge, C. J., J. E. Conel, R. O. Green, J. S. Margolis, R. G. Holm, and G. Toon, Water vapor column abundance retrievals during FIFE, *J. Geophys. Res., 97,* 18,759–18,768, 1992.

Bucholtz, A., Rayleigh-scattering calculations for the terrestrial atmosphere, *Appl. Opt., 34,* 2765–2773, 1995.

Crutzen, P. J., and M. O Andreae, Biomass burning in the tropics: Impact on atmospheric chemistry and biogeochemical cycles, *Science, 250,* 1669–1678, 1990.

Dave, J. V, and J. Gazdag, A modified Fourier transform method for multiple scattering calculations in a plane parallel Mie atmosphere, *Appl. Opt., 9,* 1457–1466, 1970.

Dubovik, O. V., T. V. Lapyonok, and S. L. Oshchepkov, Improved technique for data inversion: Optical sizing of multicomponent aerosols, *Appl. Opt., 34,* 8422–8436, 1995.

Dubovik, O. V., B. N Holben, Y. J. Kaufman, M. Yamasoe, A. Smirnov, D. Tanré, and I. Slutsker, Single-scattering albedo of smoke retrieved from sky-radiance and solar transmittance measured from ground, *J. Geophys. Res.,* this issue.

Echalar, F., P. Artaxo, J. V. Martins, M. A. Yamasoe, F. Gerab, W. Maenhaut, and B. Holben, Long-term monitoring of atmospheric aerosols in the Amazon Basin: source identification and apportionment, *J. Geophys. Res.,* this issue.

Halthore, R. N., T. F. Eck, B. N. Holben, and B. L. Markham, Sun photometric measurements of atmospheric water vapor column abundance in the 940-nm band, *J Geophys. Res., 102,* 4343–4352, 1997.

Heintzenberg, J., and M. Wendisch, On the sensitivity of cloud albedo to the partitioning of particulate absorbers in cloudy air, *Beitr Phys. Atmos., 69,* 491–499, 1996.

Hobbs, P. V., and L. F. Radke, Cloud condensation nuclei from a simulated forest fire, *Science, 163,* 279–280, 1969.

Hobbs, P. V., J. S. Reid, R. A. Kotchenruther, R. J. Ferek, and R. Weiss, Direct radiative forcing by smoke from biomass burning, *Science, 275,* 1776–1778, 1997.

Holben, B. N., A. Setzer, T. F. Eck, A. Pereira, and I. Slutsker, Effect of dry-season biomass burning on Amazon Basin aerosol concentrations and optical properties, 1992–1994, *J. Geophys. Res., 101,* 19,465–19,481, 1996.

Holben, B. N., et al., Multi-band automatic sun and sky scanning radiometer system for measurement of aerosols, in *Sixth International Symposium of Physical Measurements and Signatures in Remote Sensing, Remote Sens. Environ.,* in press, 1998.

Hudson, J. G., J. Hallett, and C. F. Rogers, Field and laboratory measurements of cloud-forming properties of combustion aerosols, *J. Geophys Res., 96,* 10,847–10,859, 1991.

Iqbal, M., *An Introduction to Solar Radiation,* Academic, San Diego, Calif., 1983.

Kasten, F., and A. T. Young, Revised optical air mass tables and approximation formula, *Appl. Opt., 28,* 4735–4738, 1989.

Kauffman, J. B., D. L. Cummings, and D. E. Ward, Relationships of fire, biomass and nutrient dynamics along a vegetation gradient in the Brazilian cerrado, *J. Ecol., 82,* 519–531, 1994.

Kaufman, Y. J., Remote sensing of direct and indirect aerosol forcing, in *Aerosol Forcing of Climate,* edited by R. J. Charlson and J. Heintzenberg, pp. 297–332, John Wiley, New York, 1995.

Kaufman, Y. J., and R. S. Fraser, The effect of smoke particles on clouds and climate forcing, *Science, 277,* 1636–1639, 1997.

Kaufman, Y. J., and T. Nakajima, Effect of Amazon smoke on cloud microphysics and albedo—Analysis from satellite imagery, *J. Appl. Meteorol., 32,* 729–744, 1993.

Kaufman, Y. J., A. Setzer, D. Ward, D. Tanré, B. N. Holben, P. Menzel, M. C. Pereira, and R. Rasmussen, Biomass burning airborne and spaceborne experiment in the Amazonas (BASE A), *J. Geophys. Res., 97,* 14,581–14,599, 1992.

Kaufman, Y. J., A. Gitelson, A. Karnieli, E. Ganor, R. S. Fraser, T. Nakajima, S. Mattoo, and B. N. Holben, Size distribution and scattering phase function of aerosol particles retrieved from sky brightness measurements, *J. Geophys. Res., 99,* 10,341–10,356, 1994.

Kaufman, Y. J., et al., The Smoke, Clouds, and Radiation-Brazil (SCAR-B) experiment, *J. Geophys. Res.,* this issue.

King, M. D., D. M., Byrne, B. M. Herman, and J. A. Reagan, Aerosol size distributions obtained by inversion of spectral optical depth measurements, *J. Atmos. Sci., 35,* 2153–2167, 1978.

Komhyr, W. D., R. D. Grass, and R. K. Leonard, Dobson spectrophotometer 83: A standard for total ozone measurements, 1962–1987, *J. Geophys. Res., 94,* 9847–9861, 1989.

Kotchenruther, R A., and P. V. Hobbs, Humidification factors of aerosols from biomass burning in Brazil., *J. Geophys. Res.,* this issue.

Kuhlbusch, T. A., and P. J. Crutzen, Black carbon, the global carbon cycle, and atmospheric carbon dioxide, in *Biomass Burning and Global Change,* vol. 1, *Remote Sensing, Modeling and Inventory Development, and Biomass Burning in Africa,* edited by J. S. Levine, pp. 160–169, MIT Press, Cambridge, Mass., 1996.

Lenoble, J., The particulate matter from biomass burning: A tutorial and critical review of its radiative impact, in *Global Biomass Burning—Atmospheric, Climatic, and Biospheric Implications,* edited by J. S. Levine, pp. 381–386, MIT Press, Cambridge, Mass., 1991.

London, J. R., D. Bojkov, S. Oltmans, and J. I. Kelley, Atlas of the global distribution of total ozone July 1957–June 1967, *NCAR Tech. Note 113 + STR,* Natl. Cent. for Atmos. Res., Boulder, Colo., 1976.

Martins, J. V., P. Artaxo, C. Liousse, J. S. Reid, P. V. Hobbs, Y. Kaufman, Effects of black carbon content, particle size, and mixing on light absorption by aerosol from biomass burning in Brazil, *J. Geophys. Res.,* this issue (a).

Martins, J. V., P. V. Hobbs, R. E. Weiss, and P. Artaxo, Sphericity and morphology of smoke particles from biomass burning in Brazil, *J. Geophys. Res.,* this issue (b).

Mishchenko, M. I., and L. D. Travis, Light scattering by polydispersions of randomly oriented spheroids with sizes comparable to wavelengths of observation, *Appl. Opt., 33,* 7206–7225, 1994.

Mishchenko, M. I., L. D. Travis, R. A. Kahn, and R. A. West, Modeling phase functions for dustlike tropospheric aerosols using a shape mixture of randomly oriented polydisperse spheroids, *J. Geophys. Res., 102,* 16,831–16,847, 1997.

Nakajima, T., and M. Tanaka, Algorithms for radiative intensity calculations in moderately thick atmospheres using a truncation approximation, *J. Quant. Spectrosc. Radiat. Transfer, 40,* 51–69, 1988.

Nakajima, T., M. Tanaka, and T. Yamauchi, Retrieval of the optical properties of aerosols from aureole and extinction data, *Appl Opt., 22,* 2951–2959, 1983.

Nakajima, T., T. Takamura, M. Yamano, M. Shiobara, T. Yamauchi, R. Goto, and K. Murai, Consistency of aerosol size distributions inferred from measurements of solar radiation and aerosols, *J. Meteorol. Soc. Jpn., 64,* 765–776, 1986.

Penner, J. E., R. J. Charlson, J. M. Hales, N. S. Laulainen, R. Leifer, T. Novakov, J. Ogren, L. F. Radke, S. E. Schwartz, and L. Travis, Quantifying and minimizing uncertainty of climate forcing by anthropogenic aerosols, *Bull. Am. Meteorol. Soc., 75,* 375–400, 1994.

Remer, L. A., Y. J. Kaufman, B. N. Holben, A. M. Thompson, and D. McNamara, Biomass burning aerosol size distribution and modeled optical properties, *J. Geophys. Res.,* this issue.

Schmid, B., and C. Wehrli, Comparison of Sun photometer calibration by use of the Langley technique and the standard lamp, *Appl. Opt., 34,* 4500–4512, 1995.

van de Hulst, H. C., *Light Scattering by Small Particles,* Dover, Mineola, New York, 1981.

Vigroux, E., Contribution a l'etude expérimentale de l'absorption de l'ozone, *Ann. Phys., 8,* 709–762, 1953.

Ward, D. E., and C. C. Hardy, Smoke emissions from wildland fires, *Environ. Int., 17,* 117–134, 1991.

Ward, D. E., R. A. Susott, J. B. Kauffman, R. E. Babbitt, D. L. Cummings, B. Dias, B. N. Holben, Y. J. Kaufman, R. A. Rasmussen, and A. W. Setzer, Smoke and fire characteristics for cerrado and deforestation burns in Brazil: BASE-B experiment, *J. Geophys. Res., 97,* 14,601–14,619, 1992.

Warner, J., and S. Twomey, The production of cloud nuclei by cane fires and the effect on cloud droplet concentration, *J. Atmos. Sci., 24,* 704–706, 1967.

Wendisch, M., and W. von Hoyningen-Huene, High speed version of the method of "successive order of scattering" and its application to remote sensing, *Beitr. Phys. Atmos., 64,* 83–91, 1991.

Wendisch, M., and W. von Hoyningen-Huene, Optically equivalent refractive index of atmospheric aerosol particles, *Beitr. Phys. Atmos., 65,* 293–309, 1992.

Wendisch, M., and W. von Hoyningen-Huene, Possibility of refractive index determination of atmospheric aerosol particles by ground-based solar extinction and scattering measurements, *Atmos. Environ., 28,* 785–792, 1994.

West, R. A., L. R. Doose, A. M. Eibl, M. G. Tomasko, and M. I. Mishchenko, Laboratory measurements of mineral dust scattering phase function and linear polarization, *J. Geophys. Res., 102,* 16,871–16,881, 1997.

Westphal, D. L., and O. B. Toon, Simulations of microphysical, radiative, and dynamical processes in a continental-scale forest fire smoke plume, *J. Geophys. Res., 96,* 22,379–22,400, 1991.

P. Artaxo and M. A. Yamasoe, Instituto de Física, Universidade de São Paulo, Caixa Postal 66318, CEP 05315-970, São Paulo, SP, Brazil. (e-mail: akemi@if.usp.br)

O. Dubovik and L. A. Remer, NASA GSFC and Science Systems and Applications Inc., Greenbelt, MD 20771.

B. N. Holben, NASA Goddard Space Flight Center, Code 923, Greenbelt, MD 20771.

Y. J. Kaufman, NASA Goddard Space Flight Center Laboratory for Atmospheres, Greenbelt, MD 20771.